Baculovirus Inhibitor of Apoptosis Functions at or Upstream of the Apoptotic Suppressor P35 To Prevent Programmed Cell Death

GULAM A. MANJI, REBECCA R. HOZAK, DOUGLAS J. LaCOUNT, AND PAUL D. FRIESEN*

Institute for Molecular Virology and Department of Biochemistry, Graduate School and College of Agricultural and Life Sciences, University of Wisconsin—Madison, Madison, Wisconsin 53706

Members of the inhibitor of apoptosis (*iap*) gene family prevent programmed cell death induced by multiple signals in diverse organisms, suggesting that they act at a conserved step in the apoptotic pathway. To investigate the molecular mechanism of *iap* function, we expressed epitope-tagged Op-*iap*, the prototype viral *iap* from *Orgyia pseudotsugata* nuclear polyhedrosis virus, by using novel baculovirus recombinants and stably transfected insect cell lines. Epitope-tagged Op-*iap* blocked both virus- and UV radiation-induced apoptosis. With or without apoptotic stimuli, Op-IAP protein (31 kDa) cofractionated with cellular membranes and the cytosol, suggesting a cytoplasmic site of action. To identify the step(s) at which Op-*iap* blocks apoptosis, we monitored the effect of Op-*iap* expression on in vivo activation of the insect CED-3/ICE death proteases (caspases). Op-*iap* prevented in vivo caspase-mediated cleavage of the baculovirus substrate inhibitor P35 and blocked caspase activity upon viral infection or UV irradiation. However, unlike the stoichiometric inhibitor P35, Op-IAP failed to affect activated caspase as determined by in vitro protease assays. These findings provide the first biochemical evidence that Op-*iap* blocks activation of the host caspase or inhibits its activity by a mechanism distinct from P35. Moreover, as suggested by the capacity of Op-*iap* to block apoptosis induced by diverse signals, including virus infection and UV radiation, *iap* functions at a central point at or upstream from steps involving the death proteases.

The baculovirus inhibitor of apoptosis (*iap*) genes were the first members of the *iap* gene family discovered (reviewed in reference 11). Homologs of *iap* have since been identified in other viruses, mammals, and insects (4, 7, 13, 15, 19, 30, 35, 40). The antiapoptotic activity of the *iap* homologs is indicated by their capacity to suppress apoptosis to various degrees when overexpressed in vertebrate and invertebrate cell cultures (12, 15, 30, 40). In addition, *iap* homologs from *Drosophila melanogaster* block programmed cell death induced by ectopic expression of *Drosophila* death genes *reaper* and *hid* within the eyes of transgenic flies (19). Furthermore, mutations in the human *iap* homolog NAIP are linked to inappropriate depletion of motor neurons associated with spinal muscular atrophy, an autosomal neurodegenerative disorder (36). Collectively, these findings suggest that *iap* normally functions to regulate programmed cell death at a conserved step in the apoptotic pathway. However, neither the affected step(s) nor the mechanism of *iap* function is known.

Virus-encoded genes have provided important insight into programmed cell death because of their capacity to intervene in the host cell death program by mimicking or regulating conserved components of the apoptotic pathway (reviewed in references 11, 14, and 43). The baculoviral *iap* homolog Op-*iap* from *Orgyia pseudotsugata* nuclear polyhedrosis virus was identified by its capacity to suppress apoptosis induced by a *p35* null mutant of *Autographa californica* nuclear polyhedrosis virus (Ac*M*NPV) (4). The predicted Op-*iap* gene product Op-IAP contains protein motifs characteristic of the IAP family, including two N-terminal domains (~70 residues) designated baculovirus IAP repeats (BIRs) and a C-terminal RING finger (Fig. 1A). Both types of motifs contain arrangements of His and Cys residues consistent with metal ion coordination and are required for antiapoptotic activity in insect cells (4, 12). Since overexpression of Op-*iap* prevents mammalian cell apoptosis induced by Sindbis virus infection or transfection with pro-(p32) interleukin 1β-converting enzyme (ICE) (15, 18, 40), it is likely that Op-*iap* also functions at a highly conserved step in the death pathway.

Current evidence suggests that apoptosis involves distinct signaling and execution phases (17, 38, 43). Diverse signals converge to activate one or more members of the conserved family of CED-3/ICE cysteine proteases (caspases) required for apoptotic death (reviewed in references 9, 26, and 31). Caspase activation involves proteolytic processing of a procaspase yielding active protease that leads to cell death including chromatin condensation, degradation of nuclear DNA, and plasma membrane blebbing (9, 17). Although little is known about regulation of the caspases, their critical role in cell death is underscored by the existence of multiple host and viral apoptotic regulators that affect either caspase activation or activity (9, 26, 31). In the case of the baculovirus apoptotic suppressor *p35* (10), stoichiometric interaction of active caspase with P35 protein blocks protease activity by a mechanism that requires P35 cleavage at residue Asp^{87} (3, 5, 44). P35's inhibition of phylogenetically diverse caspases accounts for its capacity to block programmed cell death in diverse organisms (2, 6, 10, 20, 34, 39). In wild-type Ac*M*NPV-infected *Spodoptera frugiperda* SF21 cells, inhibition of the infection-activated host caspase by P35 prevents apoptosis (3, 27).

To gain insight into the molecular mechanism of *iap* function, we first expressed epitope-tagged Op-*iap* by using novel baculovirus recombinants. This experimental strategy provided the means to test the activity of efficiently expressed Op-*iap*

* Corresponding author. Mailing address: Institute for Molecular Virology, Bock Laboratories, University of Wisconsin—Madison, 1525 Linden Dr., Madison, WI 53706-1596. Phone: (608) 262-7774. Fax: (608) 262-7414. E-mail: PFriesen@facstaff.wisc.edu.
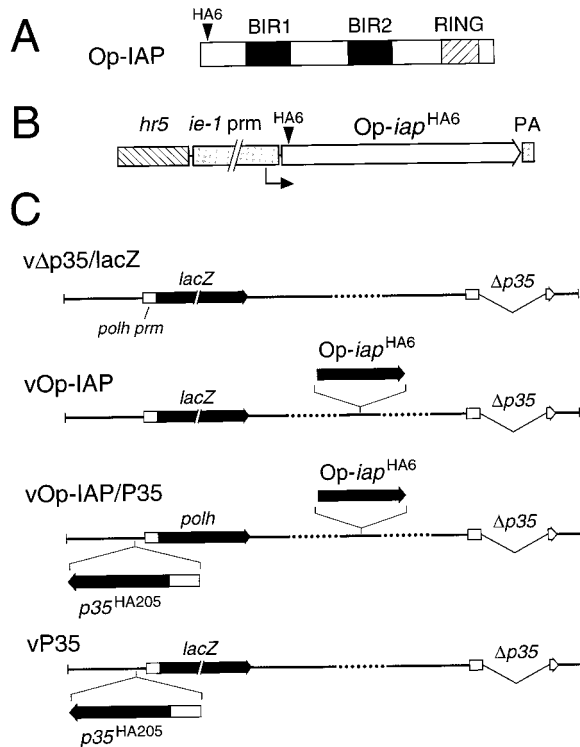
FIG. 1. (A) Op-IAP protein structure. BIR motifs (closed boxes) and the RING finger (cross-hatched) are indicated within Op-IAP (open rectangle). The 9-amino-acid HA epitope is located at residue 6. (B) Op-*iap* expression vector. The AcMNPV *ie-1* promoter (prm) and the *hr5* enhancer direct expression of Op-*iap* that precedes a polyadenylation signal (PA). The small arrow depicts the start site for transcription. (C) Gene organization of AcMNPV mutants containing Op-*iap* and *p35*. A linear representation of the 134-kbp DNA genome of AcMNPV recombinants is shown. Native *p35* was deleted (Δ*p35*) from all mutants. vΔp35/lacZ was used to generate vOp-IAP (vΔp35/lacZ/iap^{HA}) by nonhomologous integration of a single HA-tagged copy of Op-*iap*. Subsequent replacement of the vOp-IAP *lacZ* gene with *p35*^{HA205} and the polyhedrin locus generated recombinant vOp-IAP/P35 (vΔp35/iap^{HA}/p35^{HA}). vP35 (vΔp35/lacZ/p35^{HA}) contains HA-tagged *p35* inserted adjacent to *lacZ* at the polyhedrin locus.

and other apoptotic regulatory genes in cells simultaneously induced to undergo apoptosis by infection. Op-*iap*'s capacity to block apoptosis induced by different signals was tested directly by generating SF21 cells stably transfected with Op-*iap*. Using both approaches, we report here that Op-IAP is synthesized as a 31-kDa polypeptide that associates with membrane and cytosolic fractions with or without apoptotic stimuli. By using baculovirus P35 cleavage as a sensitive in vivo indicator of activated caspase, we show that Op-*iap* blocks the activation or activity of the *S. frugiperda* caspase. Confirming this conclusion, constitutive expression of Op-*iap* in SF21 cells blocked caspase activity induced by UV radiation and protected these cells from UV doses that caused apoptotic death of untransfected cells. Unlike the stoichiometric inhibitor P35, Op-IAP failed to affect in vitro caspase activity. These findings indicate for the first time that Op-IAP functions at or upstream from P35 in blocking cell death. Thus, Op-IAP likely functions during the signaling phase of apoptosis at or before caspase activation.

MATERIALS AND METHODS

Op-*iap* plasmids. Plasmid pPRM⁻IAP was constructed by inserting a 911-bp *Hin*dIII-*Cla*I fragment from the OpMNPV *Hin*dIII K genome fragment (29) into the corresponding sites of pBluescript (KS⁺) (Stratagene). A unique *Nhe*I site was inserted into pPRM⁻IAP at *iap* codon 6 by PCR-based site-directed mu-

tagenesis (8) with two pBluescript-specific primers and an *iap*-specific primer, 5′-TTGCGGCGCGCCGCGCTAGCTCGGGAGCTCATTCTG-3′ (*Nhe*I site underlined). Complementary oligonucleotides encoding the influenza virus hemagglutinin (HA) epitope YPYDVPDYA were inserted at the *Nhe*I site to generate plasmid pPRM⁻IAP^{HA}. Epitope insertion was confirmed by nucleotide sequencing. A 959-bp *Hin*dIII-*Sal*I fragment from pPRM⁻IAP^{HA} was inserted into the corresponding sites of pIE1^{hr}/PA located downstream of the *ie-1* promoter (6) to generate pIE1-IAP^{HA}/PA (Fig. 1B).

Cells and viruses. *S. frugiperda* IPL-SF21 (41) cells were propagated in TC100 growth medium (GIBCO Laboratories) supplemented with 10% heat-inactivated fetal bovine serum (HyClone Laboratories) and 2.6 mg of tryptose broth per ml. Monolayers were inoculated with budded virus according to the indicated multiplicity of infection (MOI). After 1 h, the residual inoculum was replaced with growth medium, and cells were incubated at 27°C. Wild-type AcMNPV (L-1 strain) (28), AcMNPV recombinants vΔp35 and vΔp35/lacZ (formerly vΔ35K and vΔ35K/lacZ, respectively) (22), and vΔ35K/lacZ/p35^{205} (vP35) (3) were described previously (Fig. 1C). AcMNPV vΔp35/lacZ/iap^{HA} (vOp-IAP) containing epitope-tagged Op-*iap* (Fig. 1C) was generated by gene insertion (3) in which SF21 cells were transfected with pPRM⁻IAP^{HA} and inoculated 12 h later with vΔp35/lacZ. *lacZ*-expressing (blue) recombinants were plaque purified with SF21 cells in the presence of X-Gal (5-bromo-4-chloro-3-indolyl-β-D-galactopyranoside). Southern and nucleotide sequence analyses of the purified vOp-IAP representative used here indicated that the epitope-tagged copy of Op-*iap* integrated within the *Eco*RI-G genome fragment of vΔp35/lacZ at nucleotide 73,012 (1) such that Op-*iap* transcription occurs left to right (data not shown). Recombinant vΔp35/iap^{HA}/p35^{HA205} (vOp-IAP/P35) was generated similarly, except that *lacZ* was replaced with the polyhedrin gene linked with *p35*^{HA205} (HA tagged at residue 205) at the polyhedrin locus of vOp-IAP by the approach described previously (21). Occlusion-positive, *lacZ*-deficient recombinants were plaque purified by using SF21 cells. The genotype of each virus was verified by restriction analysis of isolated viral DNA or PCR-amplified DNA fragments.

Op-*iap* stably transfected cells. SF21 cells were transfected with pIE1-IAP^{HA}/PA and pIE1/neo/PA and selected with Geneticin (G418 sulfate; GIBCO-BRL) as described previously (6). Pooled cells were generated by collecting all G418-resistant cells, whereas cloned cell lines were isolated by serial dilution of cells into 96-well culture plates. Cells were propagated in the absence of G418 after selection.

UV irradiation and DNA fragmentation assays. Parental or stably transfected SF21 cells (4 × 10⁶ per 60-mm-diameter plate) in fresh growth medium were irradiated for 10 min at room temperature by using a UV transilluminator (Fotodyne) equipped with four 8-W (312-nm) bulbs. After irradiation, cells were incubated at 27°C for 12 h, at which time, intact cells and associated apoptotic bodies were collected by centrifugation. Low-molecular-weight DNA isolated from the intact cells and associated apoptotic bodies was subjected to electrophoresis by using 2% agarose–Tris-borate-EDTA gels with ethidium bromide as described previously (22).

Immunoblot analysis. Whole-cell lysates in sodium dodecyl sulfate (SDS) were subjected to SDS-polyacrylamide gel electrophoresis and transferred to membranes. To detect HA-containing proteins, immunoblots were incubated for 1 h with a 1:250 to 1:1,000 dilution of HA-specific 12CA5 mouse monoclonal antibody (BAbCO). To detect AcMNPV gp64, immunoblots were incubated with a 1:100 dilution of gp64-specific monoclonal antibody AcV₅ (23), kindly provided by Gary Blissard (Cornell University) as the hybridoma culture supernatant. Immunoblots were subsequently incubated with a 1:3,000 to 1:10,000 dilution of goat anti-mouse immunoglobulin G (Jackson ImmunoResearch Laboratories, Inc.) conjugated to alkaline phosphatase and developed for color as described previously (22).

Subcellular fractionation. Op-*iap*-transfected cell line IAP^{F6} and SF21 cells 16 h after infection with vOp-IAP were fractionated by Dounce homogenization and differential centrifugation as described previously (22). In brief, cells were collected and disrupted in ice-cold 10 mM Tris (pH 7.5)–5 mM MgCl₂. The nuclei were separated from the S1 fraction by centrifugation (300 × g for 5 min) and pelleted through a 1.6 M sucrose cushion for 45 min at 44,000 × g (SW28.1 rotor). After a 30-min incubation in ice-cold 1% Triton X-100, the nuclei were collected by centrifugation (300 × g). The S1 fraction (see above) was subjected to centrifugation (10,000 × g for 10 min) to collect the heavy membrane fraction. The resulting supernatant (S2 fraction) was subjected to centrifugation (150,000 × g for 60 min) by using a TLA100.2 rotor to produce the light membrane pellet and the 150,000 × g cytosolic supernatant. All fractions were adjusted to 1% SDS–1% β-mercaptoethanol (βME) and boiled prior to immunoblot analysis.

***S. frugiperda* caspase-containing extracts.** SF21 cell extracts were prepared as described previously (27). In brief, intact cells and apoptotic vesicles were collected 10 h after UV irradiation or 24 h after infection with the indicated viruses. After suspension in a mixture of 10 mM HEPES (N-2-hydroxyethylpiperazine-N′-2-ethanesulfonic acid) (pH 7.0), 0.1% CHAPS {3-[(3-cholamidopropyl)-dimethyl-ammonio]-1-propanesulfonate}, 5 mM dithiothreitol, 2 mM EDTA, and protease inhibitor cocktail (Pharmingen), the cells were disrupted by one freeze-thaw cycle and Dounce homogenization. The resulting cell lysates were clarified by centrifugation (150,000 × g) for 2 h at 4°C and stored at −80°C. Protein concentrations were determined by using the Bio-Rad protein assay with bovine gamma globulin as the standard.

***S. frugiperda* caspase assays.** [^{35}S]Met-Cys-labeled P35 was synthesized in a coupled transcription-translation system (Promega Corp.) by using pSP6-35K as DNA template (3). Protease assays with in vitro-translated (IVT) P35 (0.5 μl) as substrate were performed with 20-μl reaction mixtures that contained cleavage buffer (100 mM HEPES [pH 7.5], 10% [wt/vol] sucrose, 0.1% [wt/vol] CHAPS, 10 mM dithiothreitol) and extract (20 μg of protein) from the indicated SF21 cells. After 2 h at 27°C, the reactions were adjusted to 1% SDS–1% βME and boiled. Where indicated, S2 fractions (containing cytosol and light membrane fractions) from uninfected and vOp-IAP- and vP35-infected cells were combined with *S. frugiperda* caspase-containing extract (25 μg of protein) from vΔp35-infected cells. After 2 h at 27°C, IVT P35 substrate (0.5 μl) diluted in cleavage buffer was added. After another 2 h, the reaction was boiled in 1% SDS–1% βME and subjected to electrophoresis on SDS–10 to 20% polyacrylamide gels followed by fluorography.

Image processing. Autoradiograms were scanned at a resolution of 300 dpi by using a Microtek Scanmaker III equipped with a transparency adapter. The resulting files were printed from Adobe Photoshop 2.5 by using a Tektronix Phaser IISDX dye sublimation printer.

RESULTS

Identification of Op-IAP and kinetics of synthesis. Op-*iap* was epitope tagged by insertion of an oligonucleotide encoding the influenza virus HA epitope preceding codon 6 (Fig. 1A). This N-terminal placement within Op-*iap* avoided disruption of the BIR sequences. To verify antiapoptotic activity, marker rescue was used to test the capacity of HA-tagged Op-*iap* to block virus-induced apoptosis and restore replication of Ac*M*NPV *p35* deletion mutant vΔp35/lacZ (3). In this assay, SF21 cells were transfected with HA-tagged Op-*iap* and subsequently infected with apoptosis-inducing vΔp35/lacZ. Virus recombinants containing randomly integrated Op-*iap* were readily identified by their blue plaque phenotype, resulting from the acquired capacity to block apoptosis and restore polyhedrin promoter-directed expression of *lacZ* (3, 21). By using a promoterless copy of HA-tagged Op-*iap*, nonhomologous recombination generated recombinant viruses in which *iap* expression levels were sufficient to block apoptosis. A purified representative, hereafter designated vOp-IAP (Fig. 1C), was selected for further study. vOp-IAP contains a single copy of Op-*iap* stably integrated at Ac*M*NPV nucleotide 73,012. Thus, Op-*iap* insertion occurred at a position distinct from Ac*M*NPV genes *iap*1 and *iap*2, both of which fail to suppress apoptosis induced by *p35* deletion mutants (1, 4, 12, 13).

Upon infection, vOp-IAP suppressed apoptosis as efficiently as *p35*-expressing viruses. Apoptosis induced by parental virus vΔp35/lacZ, which included membrane blebbing, cytolysis, and degradation of host DNA into oligonucleosome-sized fragments (Fig. 2A, lane 3), was not detected in vOp-IAP-infected cells (lane 4) or cells infected with *p35*-containing wild-type Ac*M*NPV and vP35 (lanes 2 and 6). Upon infection with vOp-IAP (Fig. 2B), epitope-tagged Op-IAP was synthesized as a single polypeptide of the expected size (31 kDa). Op-IAP was first detected 8 to 10 h after infection, accumulated through 18 h, and declined thereafter as shown by immunoblots with HA-specific monoclonal antiserum (lanes 4 to 12). No HA-specific proteins were detected in mock- or wild-type Ac*M*NPV-infected cells (data not shown).

Prevention of UV radiation-induced apoptosis by Op-*iap*. To further verify the antiapoptotic activity of epitope-tagged Op-*iap*, we generated stably transfected SF21 cell lines. For constitutive expression, Op-*iap* was placed under control of the *hr*5 enhancer-linked *ie-1* promoter (Fig. 1B) and cotransfected with a plasmid containing the gene coding for neomycin resistance (Neo^r). Pooled and cloned G418-resistant cell lines were isolated. Of six clonal lines tested, four (C8, E6, E12, and F6) synthesized levels of Op-IAP greater than or equal to that of pooled cells or SF21 cells infected with vOp-IAP (Fig. 3A). Only cell lines E4 and G8 synthesized little or no Op-IAP. On
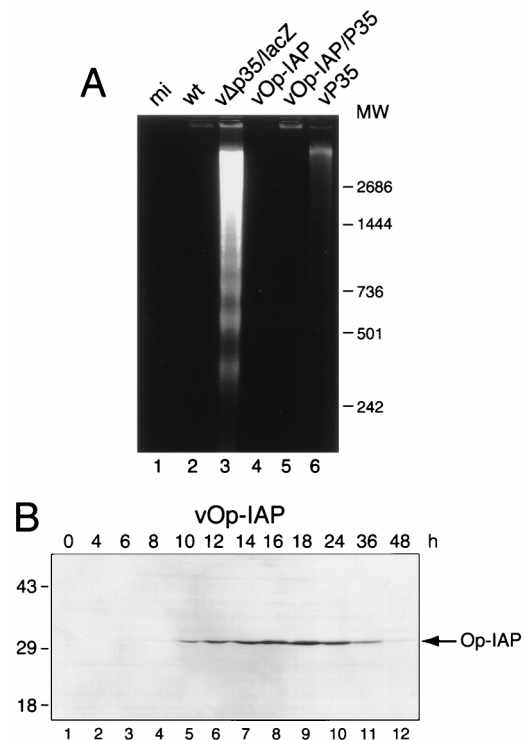
FIG. 2. Viral expression of functional Op-*iap*. (A) Virus-induced intracellular DNA fragmentation. Low-molecular-weight DNA was isolated from SF21 cells 24 h after infection with wild-type (wt) Ac*M*NPV and the indicated virus recombinants. DNA, including that from mock-infected (mi) cells, was subjected to agarose gel electrophoresis in the presence of ethidium bromide. DNA molecular weight (MW) markers (sizes in base pairs) are indicated on the right. (B) Intracellular accumulation of HA-tagged Op-IAP. SF21 cells (2 × 10^6 per plate) were lysed with SDS at the indicated times (hours) after infection with vOp-IAP (20 PFU per cell) and subjected to electrophoresis on a 5 to 20% polyacrylamide gradient gel (2.5 × 10^5 cell equivalents per lane) followed by immunoblot analysis with HA-specific monoclonal antibody 12CA5. Molecular mass markers (sizes in kilodaltons) are indicated on the left.

the basis of electrophoretic mobility, Op-IAP from stably transfected cells was indistinguishable from that of vOp-IAP-infected cells (lane 10).

DNA damage caused by UV or gamma radiation induces apoptosis in both vertebrate and invertebrate cells (reviewed in references 38 and 43). Thus, to evaluate the capacity of HA-tagged Op-*iap* to prevent programmed cell death induced by alternative signals, we tested the sensitivity of SF21 cell lines to radiation-induced apoptosis. UV radiation caused rapid and extensive apoptosis of parental SF21 cells (Fig. 4B). Membrane blebbing and apoptotic cytolysis were detected in some cells as early as 4 h after irradiation and were readily apparent in most cells by 6 to 7 h. Only 10 to 20% of the irradiated cells remained intact by 9 to 12 h (data not shown). The pattern of intracellular DNA fragmentation induced by UV radiation (Fig. 3B, lane 1) was similar to that induced by virus infection (Fig. 2A).

In contrast, stably transfected cell lines C8, E6, E12, and F6 that exhibited the highest steady-state levels of Op-IAP were protected from UV radiation-induced apoptosis. UV irradiation of these cells failed to cause apoptotic blebbing (Fig. 4D) or DNA fragmentation (Fig. 3B, lanes 5 to 8). Moreover, these cells remained viable and continued to proliferate after irradiation (data not shown). Lacking detectable Op-IAP, cell line E4 was as sensitive to UV-induced apoptosis as control Neo^r
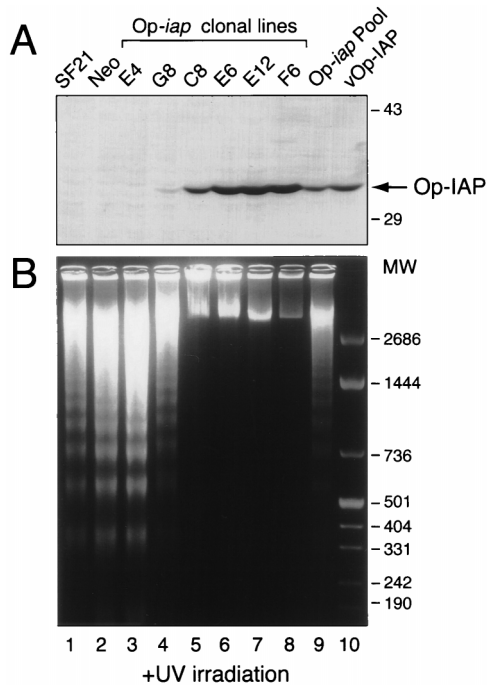
FIG. 3. Op-*iap* suppression of UV radiation-induced apoptosis. (A) Intracellular Op-IAP levels in stably transfected SF21 cells. Total cell lysates were prepared from the indicated cloned cell lines (lanes 3 to 8) or pooled cells (lane 9) and subjected to SDS-polyacrylamide gel electrophoresis (2.5×10^5 cell equivalents per lane) and immunoblot analysis by using HA-specific monoclonal antibody 12CA5. Lysates from parental SF21 cells (lane 1), cells transfected with a Neo[r] plasmid (Neo) (lane 2), and vOp-IAP-infected cells (lane 10) were included. Molecular mass markers (sizes in kilodaltons) are indicated on the right. (B) UV radiation-induced intracellular DNA fragmentation. Low-molecular-weight DNA was isolated from intact cells and associated apoptotic bodies 12 h after exposure to UV radiation (+UV) of the indicated cloned cell lines (lanes 3 to 8) or pooled cells (lane 9). DNA from parental SF21 cells (lane 1) and cells transfected with a Neo[r] plasmid (Neo) (lane 2) after UV irradiation were included. DNA molecular weight (MW) markers (lane 10) are indicated on the right (sizes in base pairs).

cells alone (Fig. 3B, lanes 2 and 3) whereas G8 with only low levels of Op-IAP showed partial protection (lane 4). Pooled Op-*iap*-transfected cells exhibited an intermediate protection, consistent with cell-to-cell variability in *iap* expression. Thus, HA-tagged Op-*iap* blocked UV-induced death in a manner dependent on the steady-state level of Op-IAP. Op-*iap* stably transfected cells were also resistant to baculovirus-induced apoptosis (24). Collectively, these data confirmed the antiapoptotic activity of this virus-derived gene.

Membrane association of Op-IAP. To examine the site of Op-IAP function, we used HA-tagged Op-*iap* to determine subcellular protein distribution. Dounce homogenates of Op-*iap*-expressing cells were biochemically fractionated by differential centrifugation. In stably transfected IAP[F6] cells, Op-IAP was detected in the cytosolic ($150,000 \times g$) supernatant and the heavy and light membrane fractions that included mitochondria, endoplasmic reticulum, and plasma membrane (Fig. 5A, lanes 2 to 4). Under the homogenization conditions used here, Op-IAP was equally distributed among these fractions. Little, if any, Op-IAP was detected in the nuclear fractions, either before or after detergent extraction (Fig. 5A, lanes 5 to 7). Although protein levels were lower, vOp-IAP-infected SF21 cells exhibited a distribution of Op-IAP between membrane and cytosolic fractions (Fig. 5B) resembling that of stably transfected cells. The identity of the subcellular fractions was

confirmed by examining the distribution of Ac*M*NPV gp64, a viral glycoprotein associated with the plasma membrane and endoplasmic reticulum (22, 33). As expected, gp64 localized to the heavy and light membrane fractions (Fig. 5C, lanes 3 and 4) but not the cytosol (lane 2). Detergent extraction of the nucleus solubilized gp64 associated with the perinuclear membrane (lanes 6 and 7). These data confirmed the direct or indirect association of Op-IAP with cellular membranes and are consistent with cytoplasmic Op-IAP function.

Inhibition of in vivo P35 cleavage by Op-IAP. To investigate the mechanism of *iap* antiapoptotic activity, we determined where Op-IAP functions in the death pathway relative to the apoptotic suppressor P35, a direct substrate inhibitor of the caspases (3, 5, 44). During baculovirus infection (3), in vivo-synthesized P35 is cleaved by a virus-activated host caspase between Asp[87]-Gly[88] to generate signature 10- and 25-kDa fragments (Fig. 6A). P35 cleavage coincides with activation of the *S. frugiperda* caspase (27) and is thus a sensitive indicator of in vivo activation of the death proteases.

To determine the effect of Op-*iap* on caspase activity during apoptotic signaling, we monitored intracellular cleavage of P35. Op-*iap* and *p35* were coexpressed by simultaneously infecting SF21 cells with vOp-IAP and vP35 containing functional, HA-tagged copies of Op-*iap* and *p35*, respectively (Fig. 1C). Full-length, uncleaved P35 and the C-terminal P35 cleavage fragment were electrophoretically distinct from Op-IAP (Fig. 6B, lanes 8 and 9). Despite the accumulation of full-length P35 upon infection with increasing multiplicities of vP35 relative to vOp-IAP, little or no P35 cleavage fragment was detected (Fig. 6B, lanes 2 to 6). Overdeveloped immunoblots (not shown) indicated trace levels of P35 cleavage at the highest ratios of vP35 to vOp-IAP, a situation in which some cells may not have been coinfected with vOp-IAP.

Thus, to ensure simultaneous expression of Op-*iap* and *p35*, we constructed Ac*M*NPV recombinant vOp-IAP/P35, in which HA-tagged *p35* under the control of its own promoter was inserted into the genome of vOp-IAP (Fig. 1C). Upon infection of SF21 cells, vOp-IAP/P35 was as efficient as vOp-IAP or wild-type Ac*M*NPV in preventing apoptosis, as judged by the lack of intracellular DNA fragmentation (Fig. 2A, lane 5), membrane blebbing, and cytolysis. Immunoblot analysis indicated that P35 and Op-IAP were both synthesized beginning 4 to 6 h after infection with vOp-IAP/P35 (Fig. 6C). Full-length P35 accumulated during infection (lanes 4 to 12), but at no time was the P35 cleavage fragment detected. In contrast, P35 cleavage was readily detected upon infection with vP35 alone (Fig. 6C, lane 1). Taken together, these data indicated that Op-*iap* prevents in vivo *S. frugiperda* caspase cleavage of P35 and thus suggest that Op-*iap* either blocks activation of the caspase proenzyme or inhibits protease activity.

Absence of *S. frugiperda* caspase activity in Op-*iap*-expressing cells. To determine the effect of Op-IAP on *S. frugiperda* caspase after apoptotic stimulation, we tested for caspase activity by using sensitive protease assays with IVT P35 as the substrate (3, 27). *S. frugiperda* caspase-containing extracts of SF21 cells induced to undergo apoptosis by infection with *p35* deletion mutant v∆p35 readily cleaved IVT P35 into the signature 10- and 25-kDa fragments (Fig. 7A, lane 5). The observed IVT P35-cleavage activity was due to active *S. frugiperda* caspase, as indicated previously by selective inhibition with the tetrapeptide aldehyde Ac-DEVD-CHO and the inability to cleave P_1(D87A)-mutated P35 (3). In contrast, extracts of SF21 cells infected with vOp-IAP failed to cleave IVT P35, as indicated by the absence of the smaller P35 cleavage fragment (Fig. 7A, lane 3). As expected, vP35-infected cell extracts also failed to cleave IVT P35 (lane 4), since the activated *S. frugi-*

SF21 - untreated

SF21 +UV

Neo^R +UV

IAP^{E6} +UV
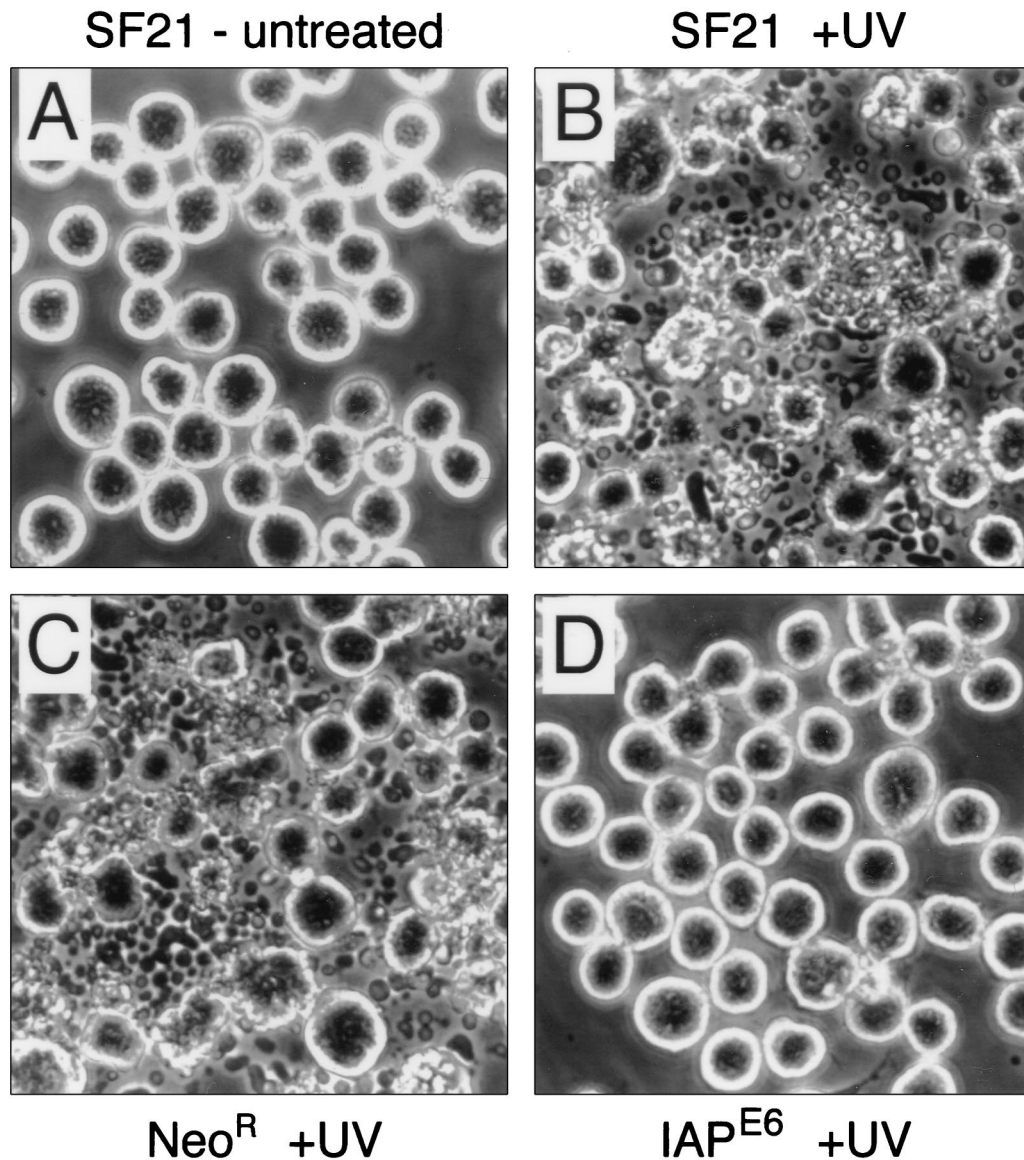
FIG. 4. UV radiation-induced apoptosis of SF21 cells. Parental SF21 cells (B), stably transfected Neo^r cells (Neo^R) (C), or cells of the Op-*iap*-transfected cell line IAP^{E6} (D) were exposed to UV radiation (+UV) and photographed 6.5 h later with a phase-contrast microscope (magnification, ×100). Nonirradiated (untreated) SF21 cells (A) are shown.

perda caspase was directly inhibited by the presence of virus-synthesized P35 (see below). Little, if any, IVT P35 cleavage was detected with extracts from mock-infected cells (lane 2).

UV radiation also caused *S. frugiperda* caspase activation, as demonstrated by IVT P35-cleavage activity within extracts of UV-irradiated, apoptotic SF21 cells (Fig. 7B, lane 5). On the basis of inhibition by DEVD-CHO but not YVAD-CHO (32), the UV-induced P35-cleavage activity was indistinguishable from that activated by baculovirus infection. In contrast, UV radiation failed to induce caspase activity in Op-*iap*-expressing cells, as demonstrated by the lack of IVT P35-cleavage activity in irradiated IAP^{F6} cell extracts (Fig. 7B, lane 4). Thus, the resistance of IAP^{F6} cells to UV-induced apoptosis correlated with the absence of active *S. frugiperda* caspase. IAP^{F6} cells exhibited no detectable caspase activity prior to irradiation (lane 2). These data indicated that Op-IAP blocks the activa-

tion or activity of *S. frugiperda* caspase induced by distinct apoptotic signals.

Failure of exogenous Op-IAP to affect active *S. frugiperda* caspase. To determine if Op-IAP inhibits *S. frugiperda* caspase by a mechanism analogous to that of the substrate inhibitor P35, we used in vitro protease assays to monitor the effect(s) of exogenous Op-IAP on *S. frugiperda* caspase activity. SF21 cell fractions consisting of light membranes and cytosol (10,000 × g supernatants) and containing Op-IAP or P35 were prepared. The presence of virus-synthesized Op-IAP and P35 was verified by immunoblot analysis (Fig. 8A, lanes 3 to 6). When active *S. frugiperda* caspase in apoptotic extracts was mixed with up to an eightfold excess of extract from mock-infected cells, no reduction in IVT P35 cleavage activity was observed (Fig. 8B, compare lane 2 to lanes 3 and 4). As expected, addition of P35-containing cell extract to the apoptotic extracts
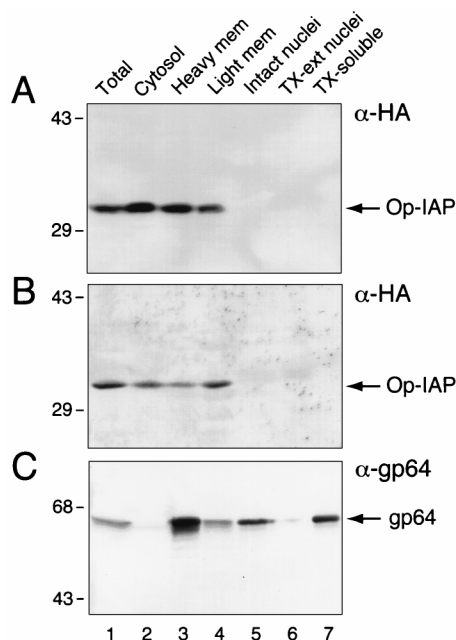
FIG. 5. Subcellular localization of Op-IAP. (A) Op-*iap* stably transfected cells. Cell line IAP[F6] was fractionated by Dounce homogenization and differential centrifugation. The resulting subcellular fractions were subjected to SDS-polyacrylamide gel electrophoresis and immunoblot analysis by using HA-specific monoclonal antibody 12CA5. (B and C) vOp-IAP-infected cells. SF21 cells were harvested 16 h after infection with vOp-IAP, fractionated, and subjected to immunoblot analysis by using HA-specific monoclonal antibody 12CA5 (α-HA) for Op-IAP detection (B) or monoclonal antiserum AcV$_5$ (α-gp64) for Ac*M*NPV gp64 detection (C). Lanes: 1, total cell protein; 2, cytosolic (150,000 × *g*) supernatant; 3, heavy membrane (mem) fraction; 4, light membrane fraction; 5, intact nuclei; 6, Triton X-100-extracted (TX-ext) nuclei; 7, Triton X-100 (TX)-soluble fraction from nuclei. Panels A and B contain 2 × 10⁶ cell equivalents per lane, and panel C contains 10⁶ cell equivalents per lane. Lane 1 contains total protein from 2.5 × 10⁵ cells. The positions of Op-IAP, gp64, and molecular mass standards (sizes in kilodaltons) are indicated.

blocked caspase activity, as indicated by the lack of IVT P35 cleavage (lanes 5 and 6). In contrast, the addition of up to an eightfold excess of Op-IAP-containing extract had no effect on caspase activity (Fig. 8B, lanes 7 and 8). Confirming this finding, 10,000 × *g* extracts from IAP[F6] cells that constitutively expressed Op-*iap* also failed to reduce *S. frugiperda* caspase activity (data not shown). Thus, unlike P35, Op-IAP exhibited no inhibitory activity towards the *S. frugiperda* caspase. Collectively, these data are consistent with Op-IAP blocking cell death at or upstream from caspase activation.

DISCUSSION

Upstream function of Op-*iap* in the programmed cell death pathway. Caspase activation is a required step in execution of apoptosis in many systems (9, 17, 42). In the case of SF21 cells, *S. frugiperda* caspase is activated by multiple signals, including baculovirus infection and UV irradiation (Fig. 9) (this report and references 3 and 27). By using functional epitope-tagged Op-*iap*, we have shown that Op-*iap* prevents the appearance of active *S. frugiperda* caspase after apoptotic stimulation. Op-*iap* blocked caspase-mediated cleavage of virus-synthesized P35 even in the presence of excess P35 (Fig. 6). Moreover, caspase activity was not detected in extracts of SF21 cells infected with vOp-IAP (Fig. 7A) or Op-*iap* stably transfected cells irradiated with UV doses that caused extensive apoptosis of untransfected cells (Fig. 7B). Thus, Op-*iap* directly or indirectly blocks
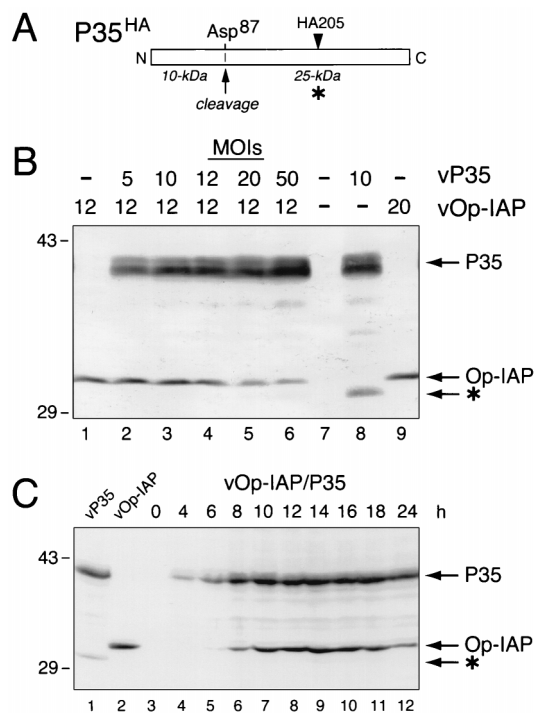
FIG. 6. Inhibition of *S. frugiperda* caspase-mediated cleavage of P35 upon expression of Op-*iap*. (A) P35[HA] structure. Caspase cleavage at P35 Asp[87] yields 10- and 25-kDa fragments; the larger cleavage fragment (∗) contains the HA tag at residue 205. (B) Coinfection with vOp-IAP and vP35. SF21 cells were infected with vOp-IAP at an MOI of 12 PFU per cell (lanes 1 to 6) and were simultaneously infected with vP35 at the indicated MOI (lanes 2 to 6). Total cell lysates (2.5 × 10⁵ cell equivalents per lane) were subjected to immunoblot analysis by using HA-specific monoclonal antibody 12CA5. Lysates from vP35-infected (lane 8) and vOp-IAP-infected (lane 9) cells only were included. (C) Infection with vOp-IAP/P35. Lysates (4 × 10⁵ cell equivalents) of SF21 cells harvested at the indicated times (hours) after infection with vOp-IAP/P35 (MOI of 20) were analyzed as described for panel B. Total lysates from cells infected with vP35 (lane 1) and vOp-IAP (lane 2) were included. Op-IAP, full-length HA-tagged P35, and the largest HA-tagged cleavage fragment of P35 (∗) are indicated. Molecular mass standards (sizes in kilodaltons) are indicated on the left.

caspase activity. P35 blocks caspase activity by functioning as a substrate inhibitor in a mechanism requiring direct interaction and P35 cleavage (3, 5, 44). Thus, the lack of caspase-mediated cleavage of intracellular P35 during infection (Fig. 6) also indicated that Op-*iap* inhibits *S. frugiperda* caspase at or upstream of *p35* in the cell death pathway (Fig. 9).

Our findings are most consistent with Op-*iap* functioning to block caspase activation during the signaling phase of apoptosis (Fig. 9). First, Op-IAP was readily detected in vOp-IAP-infected cells prior to the time (9 to 12 h) that the *S. frugiperda* caspase is activated during baculovirus infection (3, 27) and thus was present during apoptotic signaling. In addition, there is no evidence yet that Op-IAP is a direct inhibitor of activated caspase. Op-IAP-containing subcellular fractions had no effect on caspase activity in vitro, whereas direct mixing of P35 caused potent caspase inhibition (Fig. 8) (3, 5, 44). We have found no evidence of caspase-mediated cleavage of intracellular Op-IAP in protease assays, suggesting that Op-IAP is not a substrate inhibitor. Thus, Op-IAP must function by a mechanism distinct from that of P35. Determination of Op-*iap*'s effect on processing of the *S. frugiperda* procaspase(s) during apoptotic signaling will further refine the step at which Op-*iap* blocks programmed cell death.
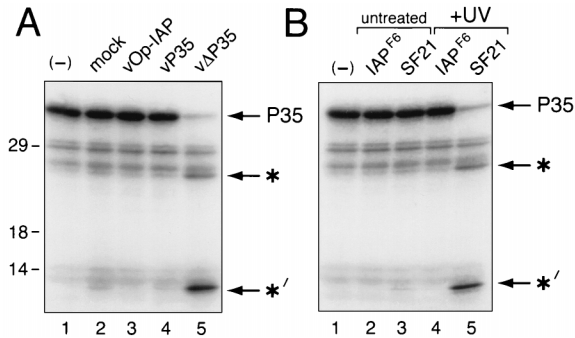
FIG. 7. Effect of Op-*iap* expression on *S. frugiperda* caspase activity. (A) IVT P35 cleavage by infected cell extracts. For protease assays, IVT [³⁵S]Met-Cys-labeled P35 was mixed with 150,000 × *g* cytosolic extracts (20 μg of protein) prepared from SF21 cells 24 h after mock infection (mock) or infection with vOp-IAP, vP35, or vΔp35/lacZ (vΔP35). After 2 h, reaction products were subjected to SDS-polyacrylamide gel electrophoresis and fluorography. (B) IVT P35 cleavage by extracts from UV-irradiated cells. Protease assays containing 150,000 × *g* cytosolic extract (20 μg of protein) from SF21 or IAP^F6 cells that were UV irradiated (+UV) or untreated were conducted as described for panel A. Lane 1 of panels A and B contains IVT P35 alone (−). Full-length P35 and the 25-kDa (∗) and 10-kDa (∗′) cleavage fragments are indicated. Because of its higher Met content, the 10-kDa fragment is more intensely radiolabeled than the 25-kDa fragment. Molecular mass markers (sizes in kilodaltons) are shown on the left.

Op-*iap* inhibition of UV radiation-induced apoptosis. The molecular mechanisms by which DNA damage engages the apoptotic machinery through p53-dependent or p53-independent pathways are largely unknown (reviewed by references 16,
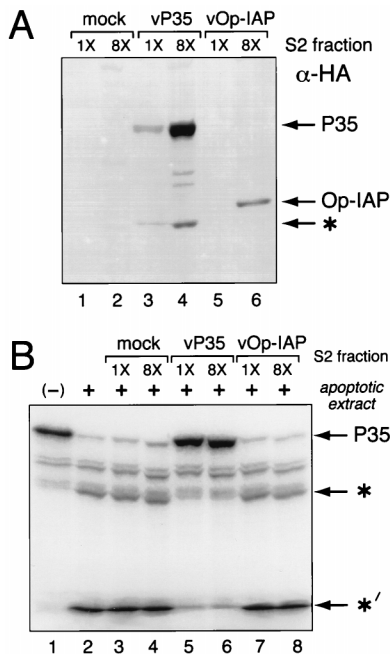
FIG. 8. Effect of exogenous Op-IAP on virus-activated *S. frugiperda* caspase. Cytosolic 10,000 × *g* extract containing 25 (1X) or 200 (8X) μg of protein from mock-, vP35-, or vOp-IAP-infected SF21 cells was mixed with 150,000 × *g* extracts (25 μg of protein) of apoptotic cells prepared 24 h after infection with mutant vΔP35. The mixture was subjected to immunoblot analysis by using HA-specific monoclonal antibody 12CA5 (A). HA-tagged Op-IAP, P35, and the largest P35 cleavage fragment (∗) are indicated. After a 2-h incubation of the mixed extracts, *S. frugiperda* caspase activity was assayed as described in the legend to Fig. 7 by using IVT ³⁵S-P35 as substrate (B). IVT P35 alone was included (lane 1). Full-length P35 and the 25-kDa (∗) and 10-kDa (∗′) fragments are indicated.
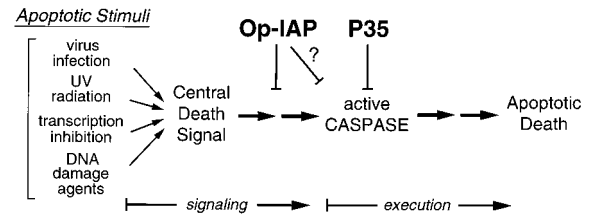
FIG. 9. Model for Op-IAP and P35 intervention in the programmed cell death pathway. SF21 cells undergo apoptosis in response to diverse signals. Apoptotic stimuli induce a centralized cell death signal that activates the proenzyme form of the *S. frugiperda* caspase(s), leading to apoptotic death. Baculovirus P35 prevents apoptosis by inhibition of active caspase through direct protease interaction. Op-IAP functions at or upstream from P35 during the signaling phase of apoptosis, to block the death caspases. Not ruled out is the possibility that Op-IAP directly inhibits activated caspase by a mechanism distinct from P35.

25, 43). UV radiation caused extensive apoptosis of SF21 cells (Fig. 3 and 4), suggesting that DNA damage can also trigger SF21 cell death. However, constitutive expression of Op-*iap* protected SF21 cells from UV-induced apoptosis (Fig. 3). This finding suggests that Op-*iap* intervenes in the death pathway triggered by DNA damage. SF21 cells were also protected from UV-induced apoptosis when stably transfected with *p35* alone (24), a finding consistent with *p35*'s downstream function. Suggestive of similar functions among the *iap*s, the *Drosophila iap* homologs DIAP1 and DIAP2 block X-ray damage-induced programmed cell death in transgenic flies (19). Thus, the *iap*s may provide additional molecular tools for defining the cellular pathways activated in response to DNA damage. The finding that Op-*iap* prevents apoptosis induced by different stimuli in SF21 cells (this report and reference 12) provides further evidence that *iap*s function at a point in the death pathway after which diverse apoptotic signals converge (Fig. 9). This conclusion is supported by the demonstrated capacity of Op-*iap* to prevent Sindbis virus- and ICE-induced apoptosis in mammalian cells (15, 18, 40) and the capacity of overexpressed cellular homologs of *iap* to prevent programmed cell death induced by other signals (15, 19, 30, 40).

Synthesis and membrane association of Op-IAP: mechanistic clues. Functional, epitope-tagged Op-IAP was detected as a single 31-kDa polypeptide in infected and stably transfected cells (Fig. 2B and 3A). Upon Dounce homogenization, about half of the intracellular Op-IAP cofractionated with heavy and light membranes of infected and stably transfected cells (Fig. 5). The lack of obvious membrane-spanning domains within Op-IAP (4) suggests that this membrane association is due to interaction with membrane-bound factors. The similar distribution of Op-IAP between membrane and cytosolic fractions in infected and uninfected cells also suggested that apoptotic signaling induced by infection does not cause a detectable redistribution of Op-IAP at the time of its peak accumulation (16 h after infection). Consistent with this conclusion was the finding that UV irradiation of Op-*iap* stably transfected cells did not alter Op-IAP subcellular distribution (data not shown). Collectively, these data suggest that Op-IAP functions in the cytoplasm in association with membranes or membrane-bound factors.

It has been recently shown that human *iap* proteins c-IAP1 and c-IAP2 interact with membrane-bound tumor necrosis factor (TNF) signal transduction complexes (35). c-IAP1 and c-IAP2 are recruited to TNF receptor 2 (TNFR2) through the association of their BIR domains with TNFR2-associated factors 1 and 2 (TRAF1 and -2). In addition, c-IAP1 and TRAF2 interact with TNFR1 in a TNF-dependent manner (37). Al-

though the physiological significance of c-IAP–TNFR interaction is unknown, these findings suggest a role for *iap* in signal transduction. Our findings here that Op-*iap* functions upstream from baculovirus *p35* to block caspase activation are consistent with a role for Op-*iap* in regulation of death signal transduction. Additional studies are required to assess the potential interaction of Op-IAP with membrane-bound signal transduction components and to determine whether viral *iap* homologs, including Op-*iap*, function in a manner analogous to those of the various cellular members of the *iap* family.

REFERENCES

1. **Ayres, M. D., S. C. Howard, J. Kuzio, M. Lopez-Ferber, and R. D. Possee.** 1994. The complete DNA sequence of *Autographa californica* nuclear polyhedrosis virus. Virology **202:**586–605.
2. **Beidler, D. R., M. Tewari, P. D. Friesen, G. Poirier, and V. M. Dixit.** 1995. The baculovirus p35 protein inhibits Fas- and tumor necrosis factor-induced apoptosis. J. Biol. Chem. **270:**16526–16528.
3. **Bertin, J., S. M. Mendrysa, D. J. LaCount, S. Gaur, J. F. Krebs, R. C. Armstrong, K. J. Tomaselli, and P. D. Friesen.** 1996. Apoptotic suppression by baculovirus P35 involves cleavage by and inhibition of a virus-induced CED-3/ICE-like protease. J. Virol. **70:**6251–6259.
4. **Birnbaum, M. J., R. J. Clem, and L. K. Miller.** 1994. An apoptosis-inhibiting gene from a nuclear polyhedrosis virus encoding a polypeptide with Cys/His sequence motifs. J. Virol. **68:**2521–2528.
5. **Bump, N. J., M. Hackett, M. Hugunin, S. Seshagiri, K. Brady, P. Chen, C. Ferenz, S. Franklin, T. Ghayur, P. Li, P. Licari, J. Mankovich, L. Shi, A. H. Greenberg, L. K. Miller, and W. W. Wong.** 1995. Inhibition of ICE family proteases by baculovirus antiapoptotic protein p35. Science **269:**1885–1888.
6. **Cartier, J. L., P. A. Hershberger, and P. D. Friesen.** 1994. Suppression of apoptosis in insect cells stably transfected with baculovirus *p35*: dominant interference by N-terminal sequences *p35*$^{1-76}$. J. Virol. **68:**7728–7737.
7. **Chacon, M. R., F. Almazan, M. L. Nogal, E. Vinuela, and J. F. Rodriguez.** 1995. The African swine fever virus IAP homolog is a late structural polypeptide. Virology **214:**670–674.
8. **Chen, B., and A. E. Przybyla.** 1994. An efficient site-directed mutagenesis method based on PCR. BioTechniques **17:**657–659.
9. **Chinnaiyan, A. M., and V. M. Dixit.** 1996. The cell death machine. Curr. Biol. **6:**555–562.
10. **Clem, R. J., M. Fechheimer, and L. K. Miller.** 1991. Prevention of apoptosis by a baculovirus gene during infection of insect cells. Science **254:**1388–1390.
11. **Clem, R. J., J. M. Hardwick, and L. K. Miller.** 1996. Anti-apoptotic genes of baculoviruses. Cell Death Differ. **3:**9–16.
12. **Clem, R. J., and L. K. Miller.** 1994. Control of programmed cell death by the baculovirus genes *p35* and *iap*. Mol. Cell. Biol. **14:**5212–5222.
13. **Crook, N. E., R. J. Clem, and L. K. Miller.** 1993. An apoptosis-inhibiting baculovirus gene with a zinc finger-like motif. J. Virol. **67:**2168–2174.
14. **Cuff, S., and J. Ruby.** 1996. Evasion of apoptosis by DNA viruses. Immunol. Cell Biol. **74:**527–537.
15. **Duckett, C. S., V. E. Nava, R. W. Gedrich, R. J. Clem, J. L. Van Dongen, M. C. Gilfillan, H. Shiels, J. M. Hardwick, and C. B. Thompson.** 1996. A conserved family of cellular genes related to the baculovirus *iap* gene and encoding apoptosis inhibitors. EMBO J. **15:**2685–2694.
16. **Enoch, T., and C. Norbury.** 1995. Cellular responses to DNA damage: cell-cycle checkpoints, apoptosis and the roles of p53 and ATM. Trends Biochem. Sci. **20:**426–430.
17. **Fraser, A., and G. Evan.** 1996. A license to kill. Cell **85:**781–784.
18. **Hawkins, C. J., A. G. Uren, G. Hacker, R. L. Medcalf, and D. L. Vaux.** 1996. Inhibition of interleukin 1-β converting enzyme-mediated apoptosis of mam-

19. **Hay, B. A., D. A. Wassarman, and G. M. Rubin.** 1995. *Drosophila* homologs of baculovirus inhibitor of apoptosis proteins function to block cell death. Cell **83:**1253–1262.
20. **Hay, B. A., T. Wolff, and G. M. Rubin.** 1994. Expression of baculovirus P35 prevents cell death in *Drosophila*. Development **120:**2121–2129.
21. **Hershberger, P. A., J. A. Dickson, and P. D. Friesen.** 1992. Site-specific mutagenesis of the 35-kilodalton protein gene encoded by *Autographa californica* nuclear polyhedrosis virus: cell line-specific effects on virus replication. J. Virol. **66:**5525–5533.
22. **Hershberger, P. A., D. J. LaCount, and P. D. Friesen.** 1994. The apoptotic suppressor P35 is required early during baculovirus replication and is targeted to the cytosol of infected cells. J. Virol. **68:**3467–3477.
23. **Hohmann, A. W., and P. Faulkner.** 1983. Monoclonal antibodies to baculovirus structural proteins: determination of specificities by Western blot analysis. Virology **125:**432–444.
24. **Hozak, R. R.** 1996. Unpublished data.
25. **Ko, L. J., and C. Prives.** 1996. P53—puzzle and paradigm. Genes Dev. **10:**1054–1072.
26. **Kumar, S.** 1995. ICE-like proteases in apoptosis. Trends Biochem. Sci. **20:**198–201.
27. **LaCount, D. J., and P. D. Friesen.** 1997. Role of early and late replication events in induction of apoptosis by baculoviruses. J. Virol. **71:**1530–1537.
28. **Lee, H. H., and L. K. Miller.** 1978. Isolation of genotypic variants of *Autographa californica* nuclear polyhedrosis virus. J. Virol. **27:**754–767.
29. **Leisy, D. J., G. F. Rohrmann, and G. S. Beaudreau.** 1984. Conservation of genome organization in two multicapsid nuclear polyhedrosis viruses. J. Virol. **52:**699–702.
30. **Liston, P., N. Roy, K. Tamai, C. Lefebvre, S. Baird, G. Cherton-Horvat, R. Farahani, M. McLean, J. E. Ikeda, A. MacKenzie, and R. G. Korneluk.** 1996. Suppression of apoptosis in mammalian cells by NAIP and a related family of IAP genes. Nature **379:**349–353.
31. **Martin, S. J., and D. R. Green.** 1995. Protease activation during apoptosis: death by a thousand cuts? Cell **82:**349–352.
32. **Mendrysa, S. M., and P. Friesen.** 1996. Unpublished data.
33. **Monsma, S. A., and G. W. Blissard.** 1995. Identification of a membrane fusion domain and an oligomerization domain in the baculovirus GP64 envelope fusion protein. J. Virol. **69:**2583–2595.
34. **Rabizadeh, S., D. J. LaCount, P. D. Friesen, and D. E. Bredesen.** 1993. Expression of the baculovirus p35 gene inhibits mammalian neural cell death. J. Neurochem. **61:**2318–2321.
35. **Rothe, M., M. G. Pan, W. J. Henzel, T. M. Ayres, and D. V. Goeddel.** 1995. The TNFR2-TRAF signaling complex contains two novel proteins related to baculoviral inhibitor of apoptosis proteins. Cell **83:**1243–1252.
36. **Roy, N., M. S. Mahadevan, M. McLean, G. Shutler, Z. Yaraghi, R. Farahani, S. Baird, A. Besner-Johnston, C. Lefebvre, X. Kang, M. Salih, H. Aubry, K. Tamai, X. Guan, P. Ioannou, T. O. Crawford, P. J. de Jong, L. Surh, J. Ikeda, R. G. Korneluk, and A. MacKenzie.** 1995. The gene for neuronal apoptosis inhibitory protein is partially deleted in individuals with spinal muscular atrophy. Cell **80:**167–178.
37. **Shu, H. B., M. Takeuchi, and D. V. Goeddel.** 1996. The tumor necrosis factor receptor 2 signal transducers traf2 and c-iap1 are components of the tumor necrosis factor receptor 1 signaling complex. Proc. Natl. Acad. Sci. USA **93:**13973–13978.
38. **Steller, H.** 1995. Mechanisms and genes of cellular suicide. Science **267:**1445–1449.
39. **Sugimoto, A., P. D. Friesen, and J. H. Rothman.** 1994. Baculovirus p35 prevents developmentally programmed cell death and rescues a ced-9 mutant in the nematode *Caenorhabditis elegans*. EMBO J. **13:**2023–2028.
40. **Uren, A. G., M. Pakusch, C. J. Hawkins, K. L. Puls, and D. L. Vaux.** 1996. Cloning and expression of apoptosis inhibitory protein homologs that function to inhibit apoptosis and/or bind tumor necrosis factor receptor-associated factors. Proc. Natl. Acad. Sci. USA **93:**4974–4978.
41. **Vaughn, J. L., R. H. Goodwin, G. J. Tompkins, and P. McCawley.** 1977. The establishment of two cell lines from the insect *Spodoptera frugiperda* (Lepidoptera; Noctuidae). In Vitro (Rockville) **13:**213–217.
42. **Vaux, D. L., G. Haecker, and A. Strasser.** 1994. An evolutionary perspective on apoptosis. Cell **76:**777–779.
43. **White, E.** 1996. Life, death, and the pursuit of apoptosis. Genes Dev. **10:**1–15.
44. **Xue, D., and H. R. Horvitz.** 1995. Inhibition of the *Caenorhabditis elegans* cell-death protease CED-3 by a CED-3 cleavage site in baculovirus p35 protein. Nature **377:**248–251.